phys. stat. sol. (a) 37, 161 (1976)
Subject classification: 7 and 14.4.1; 12.2; 20.1; 22.8.1

Physikalisches Institut der Universität Stuttgart, Teilinstitut 1

Analysis of the Acoustic Transients in the Pulse Response of the Linear Electro-Optic Effect

By
H. VEESER, U. BOGNER, and W. EISENMENGER

The pulse response of the linear electro-optic effect is investigated with high temporal and spatial resolution in KDP, KD*P, and biaxial $LiCOOH \cdot H_2O$. Experimental results, which are explained theoretically, show that the piezo-optic transients induced by the piezoelectric effect, are generated by stress release waves. Starting from the surfaces, these excite by reflection, diffraction, and superposition, due to the finite crystal dimensions, normal vibration modes too. It is shown that the direct electro-optic effect can be measured for all crystal classes at the beginning of the pulse response. The pulse method also yields static electro-optic, piezo-optic, and elastic constants. The values of r'_{63}, r_{63}, p_{66} and c_{66} measured in KDP, agree well with those of other authors. Measurement of the direct electro-optic effect of $LiCOOH \cdot H_2O$ in some directions yields values within 1 to 4×10^{-12} m/V.

Die Pulsantwortfunktion des linearen elektrooptischen Effektes wird mit hoher zeitlicher und räumlicher Auflösung an KDP, KD*P und dem optisch zweiachsigen $LiCOOH \cdot H_2O$ untersucht. Die Ergebnisse, die auch theoretisch bestätigt werden können, zeigen, daß die dabei beobachteten, piezoelektrisch erzeugten piezooptischen Phänomene von stufenförmigen Entlastungswellen herrühren, die von den Grenzflächen ausgehen, und bei deren Reflexion, Beugung und Überlagerung, infolge der endlichen Ausdehnung der Kristalle, zusätzlich mechanische Eigenschwingungen angeregt werden. Es folgt daraus, daß der direkte elektrooptische Effekt am Anfang der Pulsantwort bei allen Kristallklassen gemessen werden kann. Daneben liefert die Pulsmethode die statischen elektrooptischen, piezooptischen und elastischen Konstanten. Die an KDP gemessenen Werte von r'_{63}, r_{63}, p_{66} und c_{66} stimmen innerhalb der Meßgenauigkeit mit Werten anderer Autoren überein. Die Messung des direkten elektrooptischen Effektes von $LiCOOH \cdot H_2O$ in einigen Richtungen ergibt Werte im Bereich 1 bis 4×10^{-12} m/V.

1. Introduction

Recent theoretical and experimental investigations demonstrated that the lattice contribution to the direct (constant-strain, clamped, or high-frequency) electro-optic effect is correlated to the same non-linear properties, which also cause the Raman scatterering of transverse infrared-active optical phonons and phonon-polaritons [1 to 3]. This lattice contribution can be calculated by subtracting the pure electronic contribution obtained from optical second-harmonic generation or parametric fluorescence experiments [1] from the direct electro-optic effect. So measuring the coefficients of the direct electro-optic effect yields information about optical phonons and phonon-polaritons. The static or constant-stress electro-optic coefficients r_{ijk} include both the strain-free contribution r'_{ijk} and a contribution resulting from the piezoelectrically induced mechanical strain via the strain-optic effect:

$$r_{ijk} = r'_{ijk} + \sum p_{ijlm} d_{klm} \,. \tag{1}$$

Here p_{ijlm} are the strain-optic and d_{klm} the piezoelectric coefficients. At frequencies above mechanical resonances of the sample the crystal can no longer be

deformed uniformly and complicated high-frequency or heterodyne techniques [4] are applied to determine the strain-free electro-optic effect. In our work the pulse method is analysed, using the fact that the high-frequency electro-optic effect reacts on an abruptly applied electric field in less than 10^{-9} s due to the direct response of the electrons and the optical phonon modes. The strain-optic contribution in contrast reacts with delay, because it depends on macroscopic deformation. So far, the electro-optic pulse response has only been analysed for the special case of thin GaP bars [5]. To study the conditions which allow measurement of the linear electro-optic effect of crystals of arbitrary symmetry and dimensions by the pulse method, we analysed the electro-optic pulse response and the related solid state acoustic problem with high temporal and spatial resolution. Using the theory [6] of piezoelectric surface excitation [7], our experimental results fit the theoretical model well.

The results are also of interest for applications of the linear electro-optic effect as in frequency tuning of dye lasers by Lyot filters [8] or modulation of light intensity in Pockels cells. Several transient strain-optic phenomena observed in connection with the application of pulsed electric fields to Pockels cells [9] now find a detailed explanation.

Our experiments were carried out with uniaxial KDP and KD*P and biaxial lithium formate monohydrat (LFMH), which is of interest in non-linear optics [10], as of all nonlinear crystals so far used in second-harmonic experiments it allows generation of the shortest-wavelength ultraviolet radiation [11].

2. Experimental Method

With a 15 mW He–Ne laser, the crystal and a $\lambda/4$ plate were adjusted between polarizer and analyzer according to the Sénarmont compensation technique. The resulting light intensity is given by [12]

$$I = I_0 \sin^2\left(\varphi + \frac{\Gamma}{2}\right), \tag{2}$$

where φ is the angle between the actual and crossed analyzer positions and Γ is the electric field dependent phase difference between the ordinary and the extraordinary rays after traversing the crystal.

$$\Gamma(E) = \frac{2\pi l}{\lambda} \Delta n(E)\,, \tag{3}$$

where l is the path length in the crystal, $\Delta n(E)$ the difference of the refractive indices, and λ the laser light wavelength.

Voltage was applied to the crystal with a fast-rise pulse generator. A photomultiplier or a Si–PIN diode (rise time <0.5 ns) served as a detector. After boxcar integration the signal–time dependence was displayed by an xy recorder.

LFMH crystals were grown from saturated aqueous solutions at 42 °C by extremely slow cooling with a rate of 3 K/month. Single crystals of dimensions $2 \times 2 \times 5$ cm^3 were thus obtained without any solvent inclusions, high optical quality and high damage threshold (>500 MW/cm^2) checked by pulses of a Q-switched ruby laser. Crystal faces were polished to optical finish with diamond paste. Electrodes were evaporated semi-transparent gold layers or conductive silver paint. To avoid thermal drifting, the crystals were mounted in a thermostat.

The absolute magnitude of the electro-optic effect was measured using the Sénarmont compensator method, minimizing the transmitted intensity as observed by boxcar technique.

3. Analysis of the Electro-Optic Pulse Response

3.1 Theory

First we analyse the piezoelectrically induced elastic strains from a voltage step, starting from the fundamental equations (cf. [13])

$$T_{ij} = c_{ijkl}S_{kl} - e_{kij}E_k \quad \text{piezoelectric stress–strain ,} \tag{4}$$

$$\varrho \frac{\partial^2 u_j}{\partial t^2} = \frac{\partial T_{ij}}{\partial x_i} \quad \text{wave equation ,} \tag{5}$$

$$S_{kl} = \frac{1}{2}\left(\frac{\partial u_k}{\partial x_l} + \frac{\partial u_l}{\partial x_k}\right) \quad \text{strain definition ,} \tag{6}$$

where ϱ is the mass density, x_i the particle position vector expressed in the crystallographic coordinate system, u_j the particle displacement vector, T_{ij}, c_{ijkl}, S_{kl}, and e_{kij} the stress, stiffness, strain, and piezoelectric tensors, respectively, and E_k the value of the electric field vector. Summation over repeated indices is implied. We consider an XDP-type crystal cut parallel to the crystallographic axes (thickness a). The symmetry is $4\bar{2}m$. A [001] electric field induces the stress components T_{12} and T_{21} via the piezoelectric effect [13]. T_{12} acts in (100) planes along [010] direction and produces a displacement component $u_2(x_1)$. Similarly, T_{21} induces a displacement component $u_1(x_2)$. Since free surfaces are always planes of constant phase, u_2 is constant across the (100) faces and u_1 across the (010) faces. Neglecting first the influence of the lateral faces, i.e. the finite dimensions of the crystal, all planes parallel to the surfaces are also planes of constant phase and the calculation can be carried out one-dimensionally. Using the condensed matrix notation (equations (4) to (6)) lead to

$$\left(\frac{\partial^2}{\partial x_2^2} - \frac{1}{v^2}\frac{\partial^2}{\partial t^2}\right) u_1 = \frac{\partial}{\partial x_2} d_{36}E_3 , \tag{7}$$

$$\left(\frac{\partial^2}{\partial x_1^2} - \frac{1}{v^2}\frac{\partial^2}{\partial t^2}\right) u_2 = \frac{\partial}{\partial x_1} d_{36}E_3 \tag{8}$$

with $d_{36} = e_{36}/c_{66}$ and $v^2 = c_{66}/\varrho$. These are inhomogeneous wave equations describing plane transverse waves, where the gradient of the piezoelectric stress is the source of displacements [6]. Taking the electric field as independent of position within the crystal, the piezoelectric stress is homogeneous. So, the free (100) and (010) surfaces are sources of transverse acoustic waves, which we will call stress release waves. Equations (7) and (8) are solved by means of the Green's function method. The appropriate Green's function is [6]

$$\left.\begin{aligned} G(x, x'; t, t') &= -\frac{v}{2} \quad \text{for} \quad v(t - t') \geqq |x - x'| \quad \text{and} \quad (t - t') > 0 \\ &= 0 \quad \text{otherwise .} \end{aligned}\right\} \tag{9}$$

The [001] electric field will be taken as a step function

$$E_3(x_1, x_2, x_3, t) = E \quad \text{for} \quad 0 \leqq x_i \leqq a\,; \quad i = 1, 2, 3 \quad \text{and} \quad t \geqq 0$$
$$= 0 \quad \text{in all other cases}\,.$$

For an infinitely extended crystal $u_2(x_1, t)$ can be calculated solving the following integral

$$u_2(x_1, t) = \int G(x_1, x_1'; t, t') \frac{\partial}{\partial x_1'} E_3(x_1', t')\, \mathrm{d}x_1'\, \mathrm{d}t'\,. \tag{10}$$

The resulting strain is

$$S_{12} = \frac{1}{2}\frac{\mathrm{d}u_2}{\mathrm{d}x_1} = -\frac{d_{36}E}{4}[(-1)_1 + (1)_2 + (-1)_3 + (1)_4]\,. \tag{11}$$

The components of the summation in (11) are marked by subscripts. A component vanishes if the corresponding condition is not fulfilled.

Component 1: $x_1 \geqq 0\,; \quad vt \geqq x_1\,,$

component 2: $x_1 \leqq 0\,; \quad -vt \leqq x_1\,,$

component 3: $x_1 \leqq a\,; \quad -vt \leqq x_1 - a\,,$

component 4: $x_1 \geqq a\,; \quad vt \geqq x_1 - a\,.$

Equation (11) describes four step-like elastic waves with amplitude $d_{36}E/4$, two by two generated at the planes $x_1 = 0$ and $x_1 = a$, one of each pair travelling to the right and one to the left with velocity v.

If the planes $x_1 = 0$, and $x_1 = a$ are surfaces of a finite crystal, two of the stress release waves are immediately reflected back into the crystal without change of phase. Their strain now is added to the waves propagating into the crystal, forming waves with double amplitudes [6] which are reflected back and forth at the opposite surfaces (Fig. 1).

Similarly, equation (8) yields two plane transverse step-like waves travelling along [010] direction with the same velocity.

Consider now a LFMH crystal (point group mm2) cut parallel to its crystallographic axes. It has five non-zero piezoelectric constants (d_{31}, d_{32}, d_{33}, d_{24}, and d_{15}). A [001] electric field generates longitudinal stress components along [100], [010], and [001] directions. Neglecting the influence of the lateral surfaces equations (4) to (6) yield three uncoupled wave equations for the displacement components u_1, u_2, u_3:

$$\left(\frac{\partial^2}{\partial x_i^2} - \frac{1}{v_i^2}\frac{\partial^2}{\partial t^2}\right) u_i = \frac{\partial}{\partial x_i} d_{3i} E_3\,; \quad v_i = \sqrt{c_{ii}/\varrho} \quad \text{and} \quad i = 1, 2, 3\,. \tag{12}$$

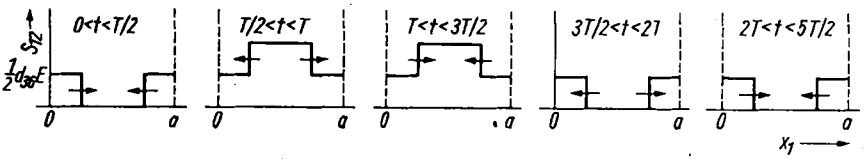

Fig. 1. Distribution of the strain S_{12} along x_1 versus time. $T = a/v$ is the travelling time of transverse elastic waves in the crystal

The solution shows that all six surfaces of the sample are sources of longitudinal plane, step-like elastic waves propagating at right angles to the surfaces with three different velocities, if the applied [001] field is also step-shaped.

For all other field directions, rectangular crystal cuts, and acentric point groups, similar solutions can be derived unless the normals of the surfaces are not directions which allow propagation of pure transverse or pure longitudinal elastic waves [13]. Strain wave solutions are then more complicated and will not be treated here.

The influence of the lateral surfaces has not been considered so far. Step-shaped elastic waves can be viewed as a superposition of sine waves of different wavelength (Fourier analysis). Plane wave propagation is a reasonable approximation for wavelengths, small compared with the crystal dimensions. However, for wavelengths comparable to them, diffraction at the edges and superposition of reflected waves lead to energy coupling into various modes of vibration [6].

In summary, the acoustic phenomena resulting from the application of a pulsed electric field can be explained as a superposition of propagating, approximately step-shaped stress release waves (short-wavelength part) and excitation of mechanical modes of vibration (long-wavelength part).

The optical signal resulting from elastic waves and vibrations depends on the strain-optic effect, described by

$$\Delta\left(\frac{1}{n^2}\right)_{ij} = p_{ijlm} S_{lm} \,, \tag{13}$$

where p_{ijlm} is the tensor of strain-optic coefficients. The phase difference in (3) is a linear function of the strain components S_{lm}. If the analyzer is turned in a position φ (equation (2)) where the variation of Γ covers a nearly linear part of the transmission function (equation (2)), the temporal variation of the strain appears nearly undistorted in the optical signal. So, with a narrow laser light beam the temporal variation of strain at each point in the cross-section of the crystal can be detected.

3.2 Experiment

Fig. 2 to 5 show electro-optic pulse response functions of a KDP cube, edge length 1 cm, cut parallel to the crystallographic axes in longitudinal configuration, i.e. electric field and light propagation are along [001] direction. Fig. 2

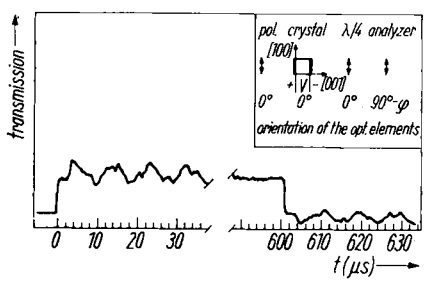

Fig. 2. Electro-optic response to a rectangular 100 V pulseP of 600 μs of a KD crystal in longitudinal configuration

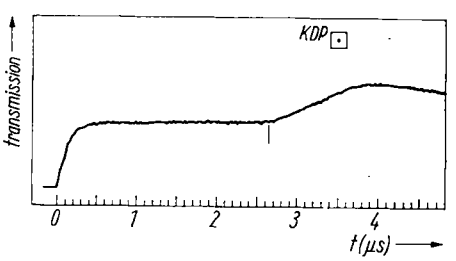

Fig. 3. Beginning of the pulse response with extended time scale. The mark indicates the onset of the strain-optic contribution resulting from a transverse wave

(insert) shows the orientation of the optical elements. If not mentioned otherwise, the laser beam passes through the centre of the crystal cross-section. Fig. 2 shows the typical response to a long rectangular voltage pulse. After a sharp rise follows a short horizontal part indicating the pure high-frequency electro-optic effect. According to the theory, after a delay of 3 μs which is exactly the time required for transverse waves to reach the laser beam in the centre of the crystal, starting from the lateral surfaces, the onset of the strain-optic contribution is observed indicating the arrival of the step-like elastic waves propagating perpendicularly to the laser beam (see also Fig. 3 in extended time scale).

After many reflections the acoustic waves decay and the static condition is reached. Switching off the electric field the same structure in the signal appears as before, but with opposite sign.

Fig. 4 shows responses to different rectangular voltage pulses with durations of even multiples of the acoustical travelling time T, the time between two reflections of transverse elastic waves at opposite surfaces. For these pulses the elastic waves generated at the beginning and at the end of the rectangular voltage pulse cancel each other. The remaining pure sine function is due to a mechanical vibration mode excited by the influence of the finite crystal dimensions. Analogously we could observe positive interference of the two successively initiated step waves at pulse durations of odd multiples of T.

In Fig. 5 the laser beam position in the cross-section has been varied. After the initial rise of the signal, one, two, three, or four steps can be observed if the laser beam is at the centre, on a diagonal, half-way between two edges or at an arbitrary point of the cross-section, respectively, because the waves propagating from each lateral surface with the same velocity reach the light beam sooner or later depending on its position. The pulse duration is an even multiple of T, so the step-like waves are extinguished after removing the field. At each position of the laser beam, only vibrational modes which agree in phase can be observed. Spatial vibration nodes could not be detected. As the amplitude decays for beam positions close to the lateral crystal faces, this oscillation can be identified with the fundamental x_1x_2 face shear [13] mode.

Fig. 6 shows the pulse response of a KD*P cube (edge length 1.8 cm) in a commercial Pockels cell with longitudinal configuration. As the electro-optic effect of KD*P is about 40% larger than that of KDP and the dimensions of

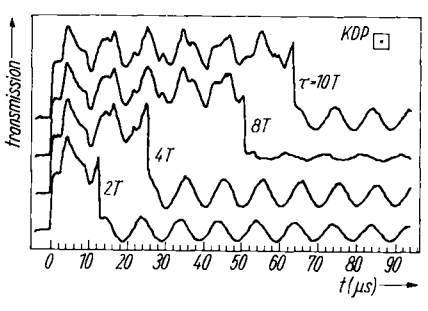

Fig. 4. Extinction of the step-like stress release waves after voltage pulses with a duration τ of even-number multiples of T

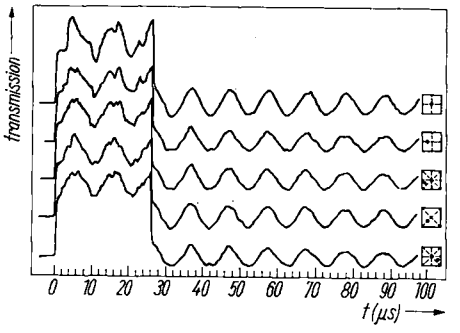

Fig. 5. Variation of the laser beam position across the crystal cross-section (indicated in the squares)

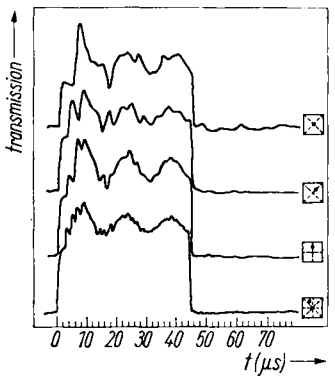

Fig. 6. Pulse response functions of KD*P in longitudinal configuration at various laser beam positions

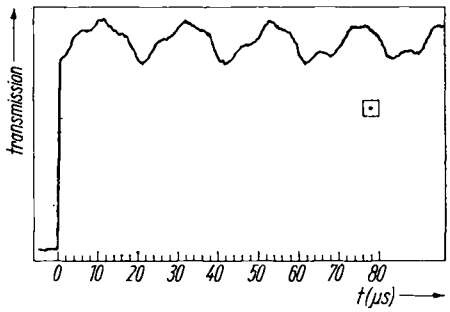

Fig. 7. Pulse response of KDP in transverse configuration

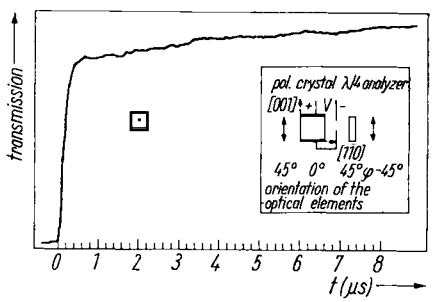

Fig. 8. Pulse response of KDP in transverse configuration

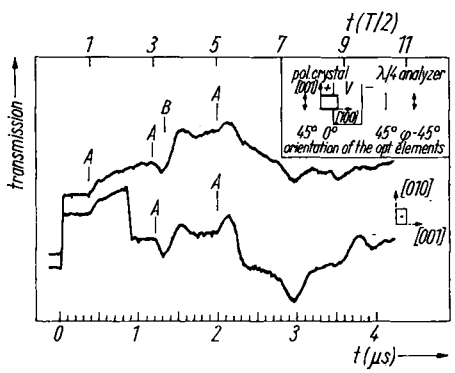

Fig. 9

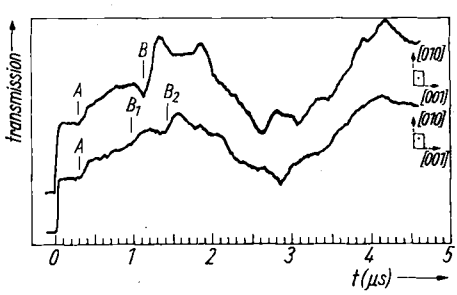

Fig. 10

Fig. 9. Pulse response of $LiCOOH \cdot H_2O$ (crystal I). Enhancement of one wave pair after pulse duration T. A, B arrival of the waves generated at the side surfaces

Fig. 10. Pulse response of $LiCOOH \cdot H_2O$ (crystal II). Laser beam in central position (upper trace) and shifted in the [010] direction. A, B arrival of the waves generated at the (001), (010) surfaces, respectively

this crystal are larger, the successively arriving step waves at non-central beam positions can be observed more clearly.

Oscillations after field switch-off are not observed, due to reduced sensitivity for small optical phase shifts according to the transmission function (2).

In Fig. 7 with a 45°-z-cut KDP of dimensions $1.0 \times 1.2 \times 2.85$ cm³ along [001], [110], and [1$\bar{1}$0] directions, the pulse response of the transverse configuration was observed. Similar considerations as above show that here a pulsed [001] field generates acoustic waves on the (110) and (1$\bar{1}$0) surfaces. As the laser beam is directed along [1$\bar{1}$0] direction, the stress release waves initiated on the (1$\bar{1}$0) planes cause, in addition to the strain-free electro-optical signal, immediately after application of the field a linear increasing strain-induced contribution which, after reflection, shows a linear decay, etc. Thus, no initial horizontal part of the signal appears. For times short compared to T, also the high-frequency electro-optic effect can be measured as the strain contribution can be neglected, as shown in Fig. 8.

Fig. 9 and 10 show the signal response of two LFMH crystals cut parallel to the crystallographic axes, with dimensions of $0.995 \times 0.52 \times 0.405$ cm³ (crystal I) and $0.77 \times 0.455 \times 0.36$ cm³ (crystal II) along [100], [010], and [001] directions. As calculated above, a pulsed [001] field generates longitudinal acoustic waves propagating along the three axes.

Fig. 9 shows the response with light propagation in [100] direction in crystal I. The onset amplitude of the high-frequency electro-optic effect is clearly resolved. The initial fast rise is followed by a short horizontal part. The contribution of the wave pair propagating parallel to the laser beam is obviously very small within this period. After 0.4 and 1.2 μs the waves (A, B) generated at the side faces arrive. We observed again that the stress release waves are enhanced or extinguished when the pulse duration is an even or odd multiple of T. The lower trace in Fig. 9 shows the response to a 0.8 μs pulse, which corresponds to T of the wave which arrives at the laser beam first. At odd multiples of $T/2$ the upper trace rises or falls. The same effects appear, enhanced below. The response of the smaller crystal II (Fig. 10) has the same structure as that of crystal I. To be able to decide which slope belongs to the waves travelling along [010] or [001], respectively, the position of the laser beam in the lower tracing of Fig. 10 was shifted along [010] direction, so that the two waves initiated at the (010) surfaces and travelling with the same velocity along the [010] direction reach the laser beam at different times. It is easily seen that the second sharp peak (B) in the upper tracing splits into two peaks (B_1, B_2), while the first peak (A) is unchanged.

4. Conclusions and Applications

Experimental and theoretical results show that the step response of the linear electro-optic effect allows measurement of the following coefficients:

1. Measuring the magnitude of the effect shortly after application of the electric field within a period which is small compared to the time between two reflections of the acoustic waves yields the pure high-frequency electro-optic coefficients.

2. After the acoustic transients have died out the coefficients of the static electro-optic effect can be measured.

3. The difference between both coefficients allows determination of piezoelectric constants if the strain-optic constants are known or vice versa via equation (1).

4. The structure of the pulse response allows measurement of the travelling time of elastic waves in the crystal, which yields the velocity of the acoustic waves and the corresponding elastic constants.

Another application of our results would be the following: At the transverse configuration of KDP a rise of the strain-optic contribution to the optical signal appeared, increasing nearly linearly in time over a few μs (see Fig. 7). An electro-optical tunable Lyot filter can be used to tune the frequency of a dye-laser emission [8]. The relatively slow rise of the birefringence according to acoustic effects as cited above, can be applied to tune a flash-lamp-pumped dye laser in the μs region by a conventional high-voltage step generator, without the necessity for the previously used high-voltage sine-wave generator [8].

5. Measured Coefficients

To test the pulse method the linear electro-optic coefficients r_{63} and r'_{63} of KDP were measured. The values are listed in Tab. 1 together with the results of other authors:

Table 1

Electro-optic coefficients
(in 10^{-12} m/V of KDP)

r_{63}	r'_{63}	ref.
10.0 ± 0.6	8.5 ± 0.4	this work
	8.8 ± 0.5	[4]
10.3 ± 0.1		[14]
10.6 ± 0.3		[15]

From $r_{63} - r'_{63} = p_{66} d_{36}$ (see equation (1)), and $d_{36} = 23.2 \times 10^{-12}$ m/V [16] we got the piezo-optic constant $p_{66} = 0.065$ in good agreement with $p_{66} = 0.0685$ given in [17]. We also obtained the elastic constant $c_{66} = (6.45 \pm 0.4) \times \times 10^{10}$ g/s^{2}cm.

After testing the pulse method with KDP it was applied to measure the unknown electro-optic effect of LFMH for three orientations. The five non-zero linear electro-optic coefficients are r_{13}, r_{23}, r_{33}, r_{42}, and r_{51} [1].

Table 2 shows the field-induced birefringence $\Delta n(E)$ and the directions of light propagation, polarization, and field for the three orientations. For the 45°-z-cut measurement a composite crystal system was required to reduce the geometrical birefringence. The indices of refraction for 633 nm light are given by Singh et al. [10].

Table 2

Field-induced $\Delta n(E)$ for specific propagation, polarization and field direction

propagation	polarization	field	field-induced $\Delta n(E)$
x_1	45° to x_3	x_3	$\frac{1}{2}(n_3^2 r_{33} - n_2^2 r_{23}) E_3$
x_2	45° to x_3	x_3	$\frac{1}{2}(n_3^2 r_{33} - n_1^2 r_{13}) E_3$
in $x_1 x_2$ plane at 45° to x_1	45° to x_3	x_3	$\frac{1}{2}[r_{33} n_3^3 - \frac{1}{2}(r_{13} + r_{23}) n_4^3] E_3$*)

*) $n_4 = \sqrt{2}\, n_1 n_2 (n_1^2 + n_2^2)^{-1/2}$.

The measured values of the high-frequency electro-optic coefficients (direct linear electro-optic effect of LFMH) for 633 nm light are given below:

$$r'_{33} - \frac{n_2^2}{n_3^2} r'_{23} = (3.8 \pm 0.3) \times 10^{-12} \frac{\mathrm{m}}{\mathrm{V}},$$

$$r'_{33} - \frac{n_1^3}{n_3^3} r'_{13} = (1.0 \pm 0.2) \times 10^{-12} \frac{\mathrm{m}}{\mathrm{V}},$$

$$r'_{33} - \frac{n_4^3}{2n_3^3}(r'_{13} + r'_{23}) = (2.2 \pm 0.15) \times 10^{-12} \frac{\mathrm{m}}{\mathrm{V}}.$$

From the pulse response functions (see Fig. 9) the strain-optic contribution at the first two orientations could be estimated. With an amount of 50 to 70% of the high-frequency effect it is relatively high compared with KDP where it is only 15%.

Taking the density $\varrho = 1.46\ \mathrm{g/cm^3}$ [18] we obtained an elastic modulus of LFMH of $c_{33} = (3.8 \pm 0.3) \times 10^{11}\ \mathrm{g/s^2cm}$ in agreement with Klapper's value $c_{33} = 4.217 \times 10^{11}\ \mathrm{g/s^2cm}$ [19].

Acknowledgements

We wish to express our gratitude to Prof. Dr. S. Haussühl for very stimulating discussions and to Fa. Zeiss/Oberkochen for supplying a KDP crystal.

References

[1] S. H. WEMPLE, Appl. Solid State Sci. **3**, 284 (1972).
[2] R. LOUDON, in: Proc. Internat. Conf. Light Scattering Spectra of Solids, Ed. G. WRIGHT, (Springer-Verlag, New York 1969 (p. 25)).
[3] W. D. JOHNSTON, JR. and I. P. KAMINOV, Phys. Rev. **188**, 1209 (1969).
W. D. JOHNSTON, JR, Phys. Rev. B **1**, 3494 (1970).
[4] R. D. ROSNER, E. H. TURNER, and I. P. KAMINOV, Appl. Optics **6**, 778 (1967).
[5] D. F. NELSON and E. H. TURNER, J. appl. Phys. **39**, 3337 (1968).
[6] E. H. JACOBSEN, J. Acoust. Soc. Amer. **32**, 949 (1960).
[7] H. BÖMMEL and K. DRANSFELD, Phys. Rev. Letters **1**, 234 (1958).
[8] H. GERLACH, Optics Commun. **8**, 41 (1973).
[9] J. M. LEY, T. M. CHRISTMAS, and C. G. WILDEY, Proc. Inst. Electr. Engng. **117**, 1057 (1970).
K. RASHIDI, Electronics Letters **7**, 115 (1970).
R. P. HILBERG and W. R. HOOK, Appl. Optics **9**, 1939 (1970).
W. D. FOUNTAIN, Appl. Optics **10**, 973 (1971).
[10] S. SINGH, W. A. BONNER, J. R. POTOPOWICZ, and L. G. VAN UITERT, Appl. Phys. Letters **17**, 292 (1970).
[11] F. B. DUNNING, F. K. TITTEL, and R. F. STEBBINGS, Optics Commun. **7**, 181 (1973).
[12] H. G. JERRARD, J. Opt. Soc. Amer. **38**, 35 (1948).
[13] W. P. MASON, Physical Acoustics, Vol. IA, Academic Press, 1966.
[14] J. H. OTT and T. R. SLIKER, J. Opt. Soc. Amer. **54**, 1442 (1964).
[15] R. S. ADHAV, J. Opt. Soc. Amer. **59**, 414 (1969).
[16] S. HAUSSÜHL, Z. Krist. **120**, 401 (1964).
[17] Landolt-Börnstein, Zahlenwerte u. Funktionen, Neue Serie, Vol. III/1, 2.
[18] A. A. CHUMAKOV and V. A. KOPTSIK, Soviet Phys. — Cryst. **4**, 214 (1960).
[19] H. KLAPPER, Z. Naturf. **28a**, 614 (1973).

(Received July 7, 1976)